ASTRODYNAMICS 2013

Volume 150

ADVANCES IN THE ASTRONAUTICAL SCIENCES

Edited by
Stephen B. Broschart
James D. Turner
Kathleen C. Howell
Felix R. Hoots

Proceedings of the AAS/AIAA Astrodynamics Specialist Conference held August 11–15, 2013, Hilton Head, South Carolina, U.S.A.

Published for the American Astronautical Society by
Univelt, Incorporated, P.O. Box 28130, San Diego, California 92198
Web Site: http://www.univelt.com

AAS Publications Office
P.O. Box 28130
San Diego, California 92198

Affiliated with the American Association for the Advancement of Science
Member of the International Astronautical Federation

First Printing 2014

Library of Congress Card No. 57-43769

ISSN 0065-3438

ISBN 978-0-87703-605-0 (Hard Cover Plus CD ROM)
ISBN 978-0-87703-606-7 (CD ROM Version)

Published for the American Astronautical Society
by Univelt, Incorporated, P.O. Box 28130, San Diego, California 92198
Web Site: http://www.univelt.com

Printed and Bound in the U.S.A.

AAS 13-772

ORBIT DETERMINATION USING NONLINEAR PARTICLE FILTER AND GPS MEASUREMENTS

Paula C. P. M. Pardal,[*] Rodolpho .V. Moraes[†] and Helio K. Kuga[‡]

A particle filter, specifically a Bayesian bootstrap filter algorithm, is applied for estimating the state vector that characterizes the orbit of a satellite, using a set of GPS measurements. The development will be evaluated through performance and computational cost, comparing the bootstrap algorithm results against the unscented Kalman filter (UKF) solution for the same problem. The orbit determination is a nonlinear problem, with respect to the dynamics and the measurements equations. It consists essentially of estimating values that completely specify the body trajectory in the space, processing a set of measurements (pseudo-ranges) related to this body. Such observations are collected through GPS receivers onboard the satellite. The bootstrap filter is proposed for implementing recursive Bayesian filters. It is a statistical, brute-force approach to estimation that often works well for systems that are highly nonlinear. Here, the bootstrap particle filter will be implemented with resampling and roughening, a scheme for combating the reduction in the number of truly distinct sample values.

INTRODUCTION

The orbit of an artificial satellite is determined using real data from the Global Positioning System (GPS) receivers. In the orbit determination process of artificial satellites, the nature of the dynamic system and the measurements equations are nonlinear. As a result, it is necessary to manage a fully nonlinear problem in which the disturbing forces as well as the measurements are not easily modeled. The variables that completely specify a satellite trajectory in the space are estimated, with the processing of a set of pseudo-range measurements related to the body.

A spaceborne GPS receiver is a powerful resource to determine orbits of artificial Earth satellites by providing many redundant measurements, which ultimately yields high degree of the observability to the problem. The Jason satellite is a nice example of using GPS for space positioning. Through an onboard GPS receiver, the pseudo-ranges (error corrupted distance from satellite to each of the tracked GPS satellites) can be measured and used to estimate the full orbital state.

The UKF is an estimator that propagates mean and covariance information through a nonlinear transformation, without needing the linearization steps [1, 2, 3]. However, the UKF is still only an approximate nonlinear estimator, and divergence will occur when nonlinearities become too severe [4]. On the other hand, the particle filter is a completely nonlinear state estimator. The boot-

[*] Dr., ICT, UNIFESP, paulacristiane@gmail.com, R. Talim, 330, São José dos Campos-SP-Brazil. CEP: 12231-280.
[†] Dr., ICT, UNIFESP, rodolpho.vilhena@gmail.com, R. Talim, 330, São José dos Campos-SP-Brazil. CEP: 12231-280.
[‡] Dr., DMC, INPE, hkk@dem.inpe.br, Av. Astronautas, 1758, São José dos Campos-SP-Brazil. CEP: 12227-010.

strap filter central idea is to express the required probability density function (pdf) as a set of random samples, instead of a function over state space [5].

In this orbit determination problem the main goal is to analyze the bootstrap filter behavior for the highly nonlinear orbit determination problem. Its simulation results are compared with the UKF for the same problem. Since the UKF application to orbit determination has been well studied [6, 7, 8], it works as a reference solution for the bootstrap filter analysis.

PARTICLE FILTER

The particle filter was designed to numerically implement the Bayesian estimator [4]. The Bayesian approach consists of constructing the pdf of the state based on all the available information, and for nonlinear or non-Gaussian problem, there is no closed form expression for the required pdf. The bootstrap filter represents the required pdf as a set of random samples, which works as an alternative to the function over state space. This filter is a recursive algorithm for propagating and updating these samples for the discrete time problem. The key update stage of the method (Bayes rules) is implemented as a weighted bootstrap [5].

The main idea of the bootstrap particle filter is intuitive and forthright. At the beginning, N particles $x_{0,i}^{+}\,(i=1,...,N)$ are randomly generated, based on the known initial pdf $p(x_0)$. At each time step k, the particles are propagated to next time step using the dynamics equation [4]. After receiving the measurement at time k, the pdf $p(y_k \mid x_{k-1}^{i})$ is evaluated. That is, the conditional relative likelihood of each particle $x_{k,i}^{-}$ is calculated. If an m-dimensional measurement equation is given as $y_k = h(x_k) + v_k$ and v_k is a Gaussian random variable with a mean of zero and a variance of R, $v_k \sim N(0,R)$, then a relative likelihood q_i that the measurement is equal to a specific measurement y^*, given the premise that x_k is equal to the particle x_{k-1}^{i}, can be computed as follow [4]:

$$\begin{aligned} q_i &= p\left(y_k = y^* \mid x_k = x_{k-1}^{i}\right) \\ &= p\left[v_k = y^* - h(x_{k-1}^{i})\right] \\ &\sim \frac{1}{(2\pi)^{m/2}\left|R\right|^{1/2}} \exp\left(\frac{-\left[y^* - h(x_{k-1}^{i})\right]^{\mathrm{T}} R^{-1}\left[y^* - h(x_{k-1}^{i})\right]}{2}\right) \end{aligned} \tag{1}$$

The ~ symbol in Equation (1) means that the probability is directly proportional to the right side. So if the equation is used for all particles $x_{k,i}^{-}$, then the relative likelihoods that the state is equal to each particle is correct. The relative likelihoods are normalized to ensure that the sum of all likelihoods is equal to one. Next, a new set of randomly generated particles $x_{k,i}^{+}$ is computed from the relative likelihoods q_i. This resampling step can be done several different ways. Here, it is used roughening, for preventing sample impoverishment. At this point, there is a set of particles $x_{k,i}^{+}$ that are distributed accordingly the pdf $p(x_k \mid y_k)$, and any desired statistical measure of it can be computed.

The particle filter, adjusted to the orbit determination problem, can be summarized as follows:

1. The dynamic and measurement equations are given as:

$$\begin{aligned} \mathbf{x}_{k+1} &= \mathbf{f}_k(\mathbf{x}_k) + \mathbf{w}_k \\ \mathbf{y}_k &= \mathbf{h}_k(\mathbf{x}_k) + \mathbf{v}_k \end{aligned} \tag{2}$$

   where $\mathbf{w}_k$ and $\mathbf{v}_k$ are independent white noise processes with known pdf's.

2. N initial particles $\mathbf{x}_{0,i}^{+}\ (i = 1,..., N)$ are randomly generated on the basis of the known initial state pdf $p(x_0)$. N is a parameter chosen as a trade-off between computational cost and estimation accuracy [4].

3. For $k = 1, 2, \ldots$:

   a. In the time propagation step, obtain a priori particles $\mathbf{x}_{k,i}^{-}$, using the dynamics equation and the pdf of the process noise, both known:

$$\mathbf{x}_{k,i}^{-} = \mathbf{f}_{k-1}(\mathbf{x}_{k-1,i}^{+}) + \mathbf{w}_{k-1}^{i} \qquad (i = 1,..., N) \tag{3}$$

   where each $\mathbf{w}_{k-1}^{i}$ noise vector is randomly generated on the basis of the known pdf of $\mathbf{w}_{k-1}$.

   b. Compute the relative likelihood q_i of each particle $x_{k,i}^{-}$, conditioned on the measurement $\mathbf{y}_k$, using the nonlinear measurement equation and the pdf of the measurement noise, as in Equation (1).

   c. Normalize the relative likelihoods:

$$q_i = \frac{q_i}{\sum_{j=1}^{N} q_j} \tag{4}$$

   d. In the resampling step, generate a set of a posteriori particles $\mathbf{x}_{k,i}^{+}$, on the basis of the relative likelihood q_i.

   e. Now there is a set of particles $\mathbf{x}_{k,i}^{+}$ distributed according to the pdf $p(x_k \mid y_k)$, $p(x_k \mid y_k)$, and mean and covariance statistical measures can be computed.

In the bootstrap filter implementation, at the start of the track and as the target approaches the observer, there is only a small overlap between the prior and the likelihood. A procedure that may be implemented for combating the consequent reduction in the number of truly distinct sample values is roughening [5]. Here, it was implemented a bootstrap particle filter with resampling (step 3.d) and roughening.

Roughening

To each sample drawn in the update (resampling) step is added an independent c_i sample from $N(0, J_k)$, where J_k is a diagonal covariance matrix. The standard deviation of the Gaussian sample corresponding to a particular component of the state is given by $\sigma = KEN^{-1/d}$, where E is the length of the interval between the maximum and the minimum samples of this component (before roughening), d is the state dimension, and K is a constant tuning parameter, chosen $K = 0.2$ [5].

UNSCENTED KALMAN FILTER (UKF)

Basically, the UKF is a nonlinear filter generated after accommodating the unscented transformation (UT) in the extended Kalman filter (EKF) algorithm. The UT is a manner of calculating the statistics of a random variable that passes through a nonlinear transformation, by selecting a suitable set of points (sigma-points) so that their mean and covariance are $\bar{\mathbf{x}}$ and $\mathbf{P}_{xx}$ respectively [2, 3]. The nonlinear function is applied to each point of the set, in turn, to yield a cloud of transformed points. The statistics of the transformed points (mean $\bar{\mathbf{y}}$ and covariance $\mathbf{P}_{yy}$) can then be calculated to form an estimate of the nonlinearly transformed mean and covariance.

The sigma-points are deterministically chosen so that they exhibit certain specific properties, and they can be weighted in ways that are inconsistent with the distribution interpretation of sample points like in the particle filter [1, 2].

The n-dimensional random variable $\mathbf{x}$, with $\bar{\mathbf{x}}$ mean and $\mathbf{P}_{xx}$ covariance, is approximated by $2n+1$ weighted points, the so known sigma-points, given by:

$$\begin{aligned} \boldsymbol{\chi}_0 &= \bar{\mathbf{x}} \\ \boldsymbol{\chi}_i &= \bar{\mathbf{x}} + \left(\sqrt{(n+\kappa)\mathbf{P}_{\mathbf{xx}}}\right)_i \\ \boldsymbol{\chi}_{i+n} &= \bar{\mathbf{x}} - \left(\sqrt{(n+\kappa)\mathbf{P}_{\mathbf{xx}}}\right)_i \end{aligned} \tag{5}$$

in which κ provides an extra degree of freedom used to fine-tune the higher order moments and is set as $\kappa = 3 - n$ for a Gaussian distribution [9]; and $\left(\sqrt{(n+\kappa)\mathbf{P}_{\mathbf{xx}}}\right)_i$ is either the i-th row or column of the square root matrix of $(n+\kappa)\mathbf{P}_{\mathbf{xx}}$. The transformation occurs as follows:

1. Transform each point through the nonlinear function to yield the set of transformed sigma points:

$$y_i = \mathbf{f}\left[\boldsymbol{\chi}_i\right] \tag{6}$$

2. The observations mean is given by the weighted average of the transformed points:

$$\bar{\mathbf{y}} = \sum_{i=0}^{2n} W_i \, y_i \tag{7}$$

3. The covariance is the weighted outer product of the transformed points:

$$\mathbf{P}_{yy} = \sum_{i=0}^{2n} W_i \left[y_i - \bar{\mathbf{y}} \right] \left[y_i - \bar{\mathbf{y}} \right]^T \tag{8}$$

W_i is the weight associated to the *i*-th point given by:

$$\begin{aligned} W_0 &= \frac{\kappa}{(n+\kappa)} \\ W_i &= \frac{1}{2(n+\kappa)}, \; i = 1,\ldots,2n \end{aligned} \tag{9}$$

The following steps are processed, in order to generate the UKF:

1. Predict the new state system and its associated covariance, taking into account the effects of the Gaussian white noise process.
2. Predict the expected observation and its residual innovation matrix considering the effects of the observation noise.
3. Predict the cross correlation matrix.

Table 1 presents an algorithm for the UKF. In the filter initialization, the mean, $\hat{\mathbf{x}}_{k-1}$, and the covariance matrix, $\hat{\mathbf{P}}_{k-1}$, of the state vector **x** are calculated, in reference to the prior instant, supposed t_{k-1}. Following, the set of sigma-points is generated, from the mean and the covariance matrix, previously calculated. In the propagation step, the generated state sigma-point set is propagated to the instant t_k, using the nonlinear dynamics equation (3.a), and the predict mean and covariance matrix are calculated (3.b). During the update cycle: the observations sigma-points are generated (4.a), propagated through the nonlinear observations equation (4.b), and its mean is obtained (4.c); the predict matrices of innovation, $\mathbf{P}_k^{vv}$, and correlation, $\mathbf{P}_k^{xy}$, are computed (4.d); and finally the Kalman gain is calculated, in order to update the state $\hat{\mathbf{x}}_k$, and the covariance matrix, $\hat{\mathbf{P}}_k$. They are used as a priori information in the next instant, t_{k+1}, to generate the new set of sigma-points.

Table 1. UKF algorithm.

1. **Initialization (t = *k*–1):**

$$\hat{\mathbf{x}}_{k-1} = E\left[\mathbf{x}_{k-1}\right] = E\left[\mathbf{x}_{k-1}^{\mathrm{T}}\mathbf{w}_{k-1}^{\mathrm{T}}\right]^{\mathrm{T}} \in \Re^{n}$$
$$\hat{\mathbf{P}}_{k-1} = E\left[(\mathbf{x}_{k-1} - \hat{\mathbf{x}}_{k-1})(\mathbf{x}_{k-1} - \hat{\mathbf{x}}_{k-1})^{\mathrm{T}}\right]$$

2. **Sigma-points:**

$$\boldsymbol{\chi}_{0,k-1} = \hat{\mathbf{x}}_{k-1}$$
$$\boldsymbol{\chi}_{i,k-1} = \hat{\mathbf{x}}_{k-1} + \left(\sqrt{(n+\lambda)\hat{\mathbf{P}}_{k-1}}\right)_i \; ; \; \boldsymbol{\chi}_{i+n,k-1} = \hat{\mathbf{x}}_{k-1} - \left(\sqrt{(n+\lambda)\hat{\mathbf{P}}_{k-1}}\right)_i$$

3. **Propagation:**

a)
$$\boldsymbol{\chi}_{0,k} = \mathbf{f}\left[\boldsymbol{\chi}_{0,k-1}\right]$$
$$\boldsymbol{\chi}_{i,k} = \mathbf{f}\left[\boldsymbol{\chi}_{i,k-1}\right], i = 1,...,2n$$

b)
$$\overline{\mathbf{x}}_k = \sum_{i=0}^{2n} W_i \, \boldsymbol{\chi}_{i,k}$$
$$\overline{\mathbf{P}}_k = \sum_{i=0}^{2n} W_i \left[\boldsymbol{\chi}_{i,k} - \overline{\mathbf{x}}_k\right]\left[\boldsymbol{\chi}_{i,k} - \overline{\mathbf{x}}_k\right]^{\mathrm{T}} + \mathbf{Q}_k$$

4. **Update:**

a)
$$\boldsymbol{\chi}_{0,k} = \overline{\mathbf{x}}_k$$
$$\boldsymbol{\chi}_{i,k} = \overline{\mathbf{x}}_k + \left(\sqrt{(n+\lambda)\overline{\mathbf{P}}_k}\right)_i \; ; \; \boldsymbol{\chi}_{i+n,k} = \overline{\mathbf{x}}_k - \left(\sqrt{(n+\lambda)\overline{\mathbf{P}}_k}\right)_i$$

b)
$$y_{0,k} = \mathbf{h}\left[\boldsymbol{\chi}_{0,k}\right]$$
$$y_{i,k} = \mathbf{h}\left[\boldsymbol{\chi}_{i,k}\right], i = 1,...,2n$$

c)
$$\overline{\mathrm{y}}_k = \sum_{i=0}^{2n} W_i \, y_{i,k}$$

d)
$$\mathbf{P}_k^{vv} = \sum_{i=0}^{2n} W_i \left[y_{i,k} - \overline{\mathrm{y}}_k\right]\left[y_{i,k} - \overline{\mathrm{y}}_k\right]^{\mathrm{T}} + \mathbf{R}_k$$
$$\mathbf{P}_k^{xy} = \sum_{i=0}^{2n} W_i \left[\boldsymbol{\chi}_{i,k} - \overline{\mathbf{x}}_k\right]\left[y_{i,k} - \overline{\mathrm{y}}_k\right]^{\mathrm{T}}$$

e)
$$\mathcal{K}_k = \mathbf{P}_k^{xy}\left(\mathbf{P}_k^{vv}\right)^{-1}$$
$$\hat{\mathbf{x}}_k = \overline{\mathbf{x}}_k + \mathcal{K}_k\left(\mathbf{y}_k - \overline{\mathrm{y}}_k\right)$$
$$\hat{\mathbf{P}}_k = \overline{\mathbf{P}}_k - \mathcal{K}_k \, \mathbf{P}_k^{vv} \, \mathcal{K}_k^{\mathrm{T}}$$

ORBIT DETERMINATION

The orbit determination is a process for obtaining values of the parameters that completely specify the motion of an orbiting body (an artificial satellite), based on a set of observations of the body. It involves nonlinear dynamical and nonlinear measurement systems, which depends on the tracking system and the estimation technique (for instance, Kalman filter or least squares methods [10, 11]). The dynamical system model consists of describing satellite orbital motion, measurements models, Earth's rotation effects, and perturbation models. These models depend on the state variables defining the initial conditions, as well as a variety of parameters which affect both the dynamic motion as the measurement process [12]. Due to the complexity of the applied models it is hardly possible to solve such models equations directly for any of these parameters from a given set of observations.

The observation may be obtained from the ground station networks using laser, radar, Doppler, or by space navigation systems, as the Global Positioning System (GPS). The choice of the tracking system depends on a compromise between the goals of the mission and the available tools. In the case of the GPS, the advantages are global coverage, high precision, low cost, and autonomous navigation resources. The GPS may provide orbit determination with accuracy at least as good as methods using ground tracking networks. The later provides standard precision around tens of meters and the former can provide precision as tight as some centimeters. The GPS provides, at a given instant, a set of many redundant measurements, which makes the orbit position observable geometrically.

After some advances of technology, the single frequency GPS receivers provide a good basis to achieve fair precision at relatively low cost, still attaining the accuracy requirements of the mission operation. The GPS allows the receiver to determine its position and time geometrically anywhere at any instant with data from at least four satellites. The principle of navigation by satellites is based in sending signals and data from the GPS satellites to a receiver located onboard the satellite that needs to have its orbit determined. This receiver measures the travel time of the signal and then calculates the distance between the receiver and the GPS satellite. Those measurements of distances are called pseudo-ranges, as shown in Figure 1.

The instantaneous orbit determination using GPS satellites is based on the geometric method. In such method, the observer knows the set of GPS satellites position in a reference frame, obtaining its own position in the same reference frame. Figure 1 illustrates the basic parameters for user position determination: $\mathbf{R}_{\mathrm{GPS}i}$ is the position of i-th GPS satellite in the reference system; $\boldsymbol{\rho}_i$ is the pseudo-range; and $\mathbf{r}_u$ is the user position in the reference system.

However, sequential orbit determination makes use of the orbital motion modeling to predict between measurement times and measurement model to update the orbit by processing of measurements from GPS. This gives rise to recursive and real time KF estimator for the orbit determination [13].

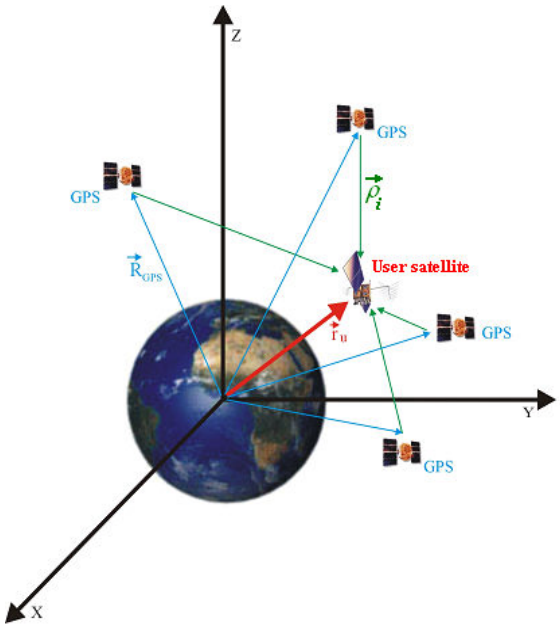

Figure 1. The geometric method for orbit determination using GPS.

Orbital Dynamic Model

In the case of orbit determination via GPS, the ordinary differential equations which represent the dynamic model are, in its simplest form, traditionally given as follows:

$$\begin{aligned} \dot{\mathbf{r}} &= \mathbf{v} \\ \dot{\mathbf{v}} &= -\mu \frac{\mathbf{r}}{\mathrm{r}^3} + \mathbf{a} + \mathbf{w}_v \\ \dot{\mathbf{b}} &= \mathrm{d} \\ \dot{\mathrm{d}} &= 0 + \mathrm{w}_\mathrm{d} \end{aligned} \tag{10}$$

wherein the variables are placed in the inertial reference frame. In Equation (10), **r** is the vector of the position components (x, y, z); **v** is the velocity vector; **a** represents the modeled perturbing accelerations; $\mathbf{w}_v$ is the white noise vector with covariance **Q**; b is the user satellite GPS clock bias; d, the user satellite GPS clock drift; and $\mathrm{w_d}$ the noise associated with the GPS clock. The GPS receiver clock offset was not taken into account, so as not to obscure the conclusions drawn in this paper due to introduction of clock offset models in the filters. Indeed, the receiver clock offset was beforehand obtained and used to correct the GPS measurements, so that the measurements are free from the error derived from receiver clock offset.

Force Model

The main disturbing forces of gravitational nature that affect the orbit of an Earth's artificial satellite are: the non-uniform distribution of Earth's mass; ocean and terrestrial tides; and the gravitational attraction of the Sun and the Moon. There are also the non-gravitational effects, such as: Earth atmospheric drag; direct and reflected solar radiation pressure; electric drag; emissivity effects; relativistic effects; and meteorites impacts.

The disturbing effects are in general included according to the physical situation presented and to the accuracy that is intended for the orbit determination. Here it was included a set of perturbations which enables to analyze the performance of the particle filter: geopotential; direct solar radiation pressure; and third body point mass effect of Sun and Moon.

Geopotential

The Earth is not a perfect sphere with homogeneous mass distribution, and cannot be considered as a material point. Such irregularities disturb the orbit of an artificial satellite and the keplerian elements that describe the orbit do not behave ideally. The geopotential function can be given by [14]:

$$U(\mathrm{r},\phi,\lambda) = \frac{\mu}{r}\sum_{n=0}^{\infty}\sum_{m=0}^{n}\left(\frac{R_\mathrm{T}}{\mathrm{r}}\right)^n P_{nm}(\sin\phi)\left(C_{nm}\cos m\lambda + S_{nm}\sin m\lambda\right) \tag{11}$$

where μ is Earth gravitational constant; $\mathrm{R_T}$ is mean Earth radius; r is the spacecraft radial distance; ϕ is the geocentric latitude; λ is the longitude on Earth fixed coordinates system; C_{nm} and S_{nm} are the harmonic spherical coefficients of degree n and order m; P_{nm} are the associated Legendre functions. The constants μ, $\mathrm{R_T}$, and the coefficients C_{nm}, and S_{nm} determine a particular gravitational potential model.

Direct Solar Radiation Pressure

The intricate direct solar radiation pressure (SRP) model applied to Jason-2 satellite is based on its geometry and is briefly described. Jason-2 is presented in Figure 2 [15].

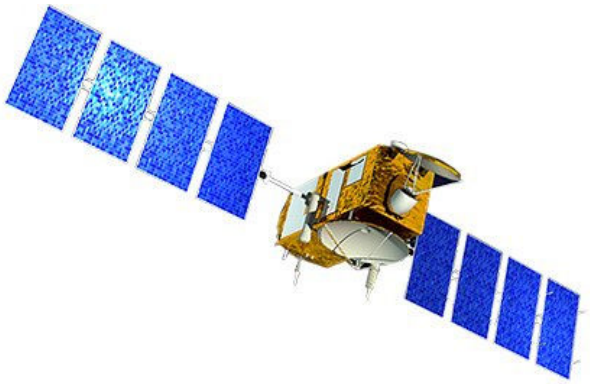

Figure 2. Jason-2 satellite.

The SRP is a force of non-gravitational origin that causes perturbations in the motion of an artificial satellite. Direct or reflected SRP is engendered throughout a continuous flux of photons that stumble at satellite surface, which can partially or totally absorb and reflect such flux.

The way the perturbations due to SRP will affect the keplerian elements depends on the pressure model adopted (if it includes or not shadow, for example). Meanwhile, in the general case, it causes secular and periodic perturbations on the angular variables (Ω, ω, and M) and periodic perturbations on the metric variables (a, e, and i).

The components of SRP force can be expressed in several systems. Throughout these systems, the orbital elements of the satellite can be connected with Sun's position. This procedure was used for the direct SRP model adopted for Jason-2. Since the force due to the emerging radiation flux on the surface of the satellite depends on the angle of incidence, the attitude of the satellite must be also taken into account [16].

According to Marshall and Luthcke's model [17], the total force acting on Jason-2 is:

$$\mathbf{F}_k = \frac{GA_k \cos\theta_k}{c}\left[2\left(\frac{\delta_k}{3} + \rho\cos\theta_k\right)\hat{n}_k + (1-\rho_k)\hat{s}\right] \Rightarrow \qquad \mathbf{F} = \sum_{k=1}^{10}\mathbf{F}_k \tag{12}$$

where G is the solar radiant flux (W/m^2); A is the surface area of each plate (m^2); δ is the diffusive reflectivity, percentage of the total incoming radiation; ρ is the specular reflectivity, percentage of the total incoming radiation; $\hat{n}$ is the surface normal vector; $\hat{s}$ is the source incidence vector; θ is the angle between surface normal and solar incidence; and c is the speed of light (m/s). Subscript k varies from 1 to 10, representing each plate of the adopted box-wing approximating model, and **F** is the total direct SRP acting on the satellite.

Sun-Moon Gravitational Attraction

Another gravitational perturbation source is that due to the Sun and the Moon attraction. They are more meaningful at farther distance from Earth. As the orbital variations are of the same type, be the Sun or the Moon the attractive body, they are normally studied without distinguishing the third body. The Sun-Moon gravitational attraction mainly acts on node and perigee causing precession of the orbit and on the orbital plane. The general three-body problem model is here simplified to the circular restricted three-body problem. In this problem, the orbital motion of a third body (a satellite, which mass can be neglected), around two other massive bodies is studied. The force that acts on the satellite, in the inertial reference frame, can be expressed as [18, 19]:

$$\ddot{\mathbf{r}}_3 = -Gm_1 \frac{\mathbf{r}_{13}}{\mathrm{r}_{13}^3} - Gm_2 \frac{\mathbf{r}_{23}}{\mathrm{r}_{23}^3} \tag{13}$$

where $\mathbf{r}_{13} = \mathbf{r}_3 - \mathbf{r}_1$, $\mathbf{r}_{23} = \mathbf{r}_3 - \mathbf{r}_2$, and $\mathbf{r}_i$, $i = 1, 2, 3$ corresponds to the i-th body distance vector to the center of mass of the system; and m_1 and m_2 are the masses of the Sun and the Moon, respectively.

Observations Model

The nonlinear equation of the observation model is

$$\mathbf{y}_k = \mathbf{h}_k(\mathbf{x}_k, \mathrm{t}) + \mathbf{v}_k \tag{14}$$

where, at time t_k, $\mathbf{y}_k$ is the vector of m observations; $\mathbf{h}_k(\mathbf{x}_k)$ is the nonlinear function of state $\mathbf{x}_k$, with dimension m; and $\mathbf{v}_k$ is the observation errors vector, with dimension m and covariance $\mathbf{R}_k$. For the present application, the ion-free pseudo-range measurements from the Jason-2 GPS receiver are used. Also, the receiver clock offset was computed before and used to correct the pseudo-range measurements. Additionally, the nonlinear pseudo-range measurement was modeled according to (Reference 20).

RESULTS

The tests and the analysis for the bootstrap filter and the UKF algorithms are presented. To validate and to analyze the methods, real GPS data from the Jason-2 satellite are used. Ocean Surface Topography Mission (OSTM)/Jason-2 is a follow-on altimetric mission to the very successful TOPEX/Poseidon mission and Jason-1. It is a joint mission between NASA and CNES (French space agency), launched June 20, 2008. Jason-2 has a repeat period of approximately 10 days with 254 passes per cycle. Its nodal period is 6,745.72 sec. Sometimes there may be anomalous or missing data. Occasionally Jason-2 must perform maneuvers to maintain orbit. When the satellite detects something abnormal it will go into safehold and will turn off all instruments and no data will be collected [21].

The filters estimated position and velocity are compared with Jason-2 precise orbit ephemeris (POE) from JPL/NASA. The test conditions consider real ion-free pseudo-range data, collected by the GPS receiver onboard Jason-2, on October 22nd, 2010, presenting up to 12 GPS satellites tracked. The tests were limited to 5.5 hours of GPS data spaced 10s. After that there was an undesirable data gap which could spoil the test case, Such 5.5 hours arc (near 3 Jason-2 orbital period) was considered sufficient for evaluating the bootstrap particle filter in this orbit determination application.

The force model comprises perturbations due to: geopotential up to order and degree 50x50; direct solar radiation pressure; and Sun-Moon gravitational attraction. This model of forces is suitable for implementation in orbit determination because of the low computational cost added compared to the improvement in the results accuracy [7, 22, 23]. The pseudo-range measurements were corrected to the first order with respect to ionosphere.

This work is not a search for results accuracy. It aims at analyzing the application of a bootstrap filter to the orbit determination problem. The analysis is based on comparing the errors in position (translated to the orbital radial, normal, and along-track RNT components) with the UKF solution. The RNT system interpretation is straightforward: the radial component "R" points to the nadir direction, the normal "N" is perpendicular to orbital plane, and the transversal (along-track) "T" is orthogonal to "R" and "N", and so is also the velocity component. Thus, it is possible to analyze what happens with the orbital RNT components and with the orbit evolution as well. There is also interest for processing time, in order to analyze the computational efforts face to the accuracy achieved by each algorithm.

Regarding time of processing, t_{CPU}, it was expected that the time required for the PF algorithm was greater than the UKF, since, even now it is the PF computational burden that is its principal obstacle to more widespread use. According to the estimator nature, each element of the state will be replaced by a certain array. The UKF uses $2n+1$ (n is the state dimension) sigma-points in place of each state variable while the PF use N particles, where N is a trade-off between computational cost and estimation accuracy. Here, the state dimension is n = 8, so 17 sigma-points were generated; while for the PF, tests were done for 17, 100, and 500 particles.

The PF first case of test was N = 17 because it is equal to the 17 sigma-points generated by the UKF, although the estimators approach is completely different. As shown in Table 2, for 17 particles, the PF was 1.7 times longer than the UKF for the processing, and the number of particles is the same as the number of sigma-points. In the case N = 100, the time of processing was 5.6 times greater than the PF (N = 17) and 10 times greater than the UKF. For N = 500, the PF was 5 times longer than the PF (N = 100), 28.8 times longer than the PF (N = 17), and 49 times longer than the UKF for processing the data. The increase in the number or particles is about 5.9 times from 17 to 100 particles; 5 times from 100 to 500; and around 29.4 times from 17 to 500. The CPU time and the increase in the number of particles show that the time of processing is related to the chosen number of particles only when the number of particles changes, but has no relation with the estimator implemented.

Table 2. Time of processing.

Estimator	t_{CPU}
UKF (17 s-p)	27 sec
PF (N = 17)	46 sec
PF (N = 100)	4 min 19 sec
PF (N = 500)	22 min 02 sec

For computing time of processing and for all the simulations shown, it was used a computer Intel ® Core ™ i5-2430M processor of 2.40 GHz, with 2.70 GB of RAM. The program was coded in FORTRAN 77 within Windows XP operating system and Compaq Visual Fortran version 6.1 compiler.

As said before, the number of particles is chosen as a trade-off between computational cost and estimation accuracy. The results in Table 3 confirms that the greater the number of particles, the better the estimation accuracy. Mean and standard deviation of the errors in RNT components were evaluated in 4 implementations: UKF; PF (N = 17); PF (N = 100); PF (N = 500). The best result was achieved by the UKF algorithm, and the PF closest performance was obtained in the PF (N = 500) version. If only the statistics are analyzed, it is clear that the estimation accuracy improves as the number of particles increases. The largest standard deviation occurred for the PF (N = 17). In the along-track component was detected a divergence occurrence, that disappeared when N was increased. For N = 100, the standard deviation was around 20m in each component, with a larger scattering between 1 and 3 hours of processing. When N = 500, the statistics and the errors behavior were very similar to the UKF solution.

Table 3. Mean and standard deviation statistics of the RNT errors.

Estimator	Radial (m)	Normal (m)	Along-track (m)
UKF (17 s-p)	- 4.07 ± 11.02	- 1.23 ± 4.05	- 0.17 ± 2.97
PF (N = 17)	- 41.46 ± 77.29	- 8.65 ± 67.83	- 546.47 ± 540.16
PF (N = 100)	- 1.48 ± 22.43	8.10 ± 25.65	4.68 ± 23.95
PF (N = 500)	- 4.02 ± 12.43	- 1.37 ± 4.22	0.85 ± 3.28

Even though a particular configuration of the PF has reached equivalent performance to the UKF, Table 2 shows a high computational effort of this PF version (22 min for 5.5h of data). These results represent the PF first experiment and, likewise the Kalman filter, it has many variants and can be tuned. This means that adjusts might be done in order to improve its efficiency. Around 100 particles should be suitable for orbit determination implementations, as long as the performance remains similar to the UKF, because the CPU time is 4 min for 5.5h of processing, according to Table 2.

In order to show the behavior of the errors in terms of RNT coordinates, Figures 3, 4 and 5 are presented. Figure 3 shows the solution obtained in UKF, which is similar to the PF (N = 500) and, for this reason, PF (N = 500) results were suppressed. Figure 4 presents the worse results, obtained when the PF (N = 17) was implemented. The errors decreases considerably for the PF (N = 100) implementation, despite an incongruous behavior between 1 and 3 hours of processing, which the PF recovers later, as can be seen in Figure 5. In these graphics, dark blue curves correspond to radial component; green, to normal; and gray, to along-track.

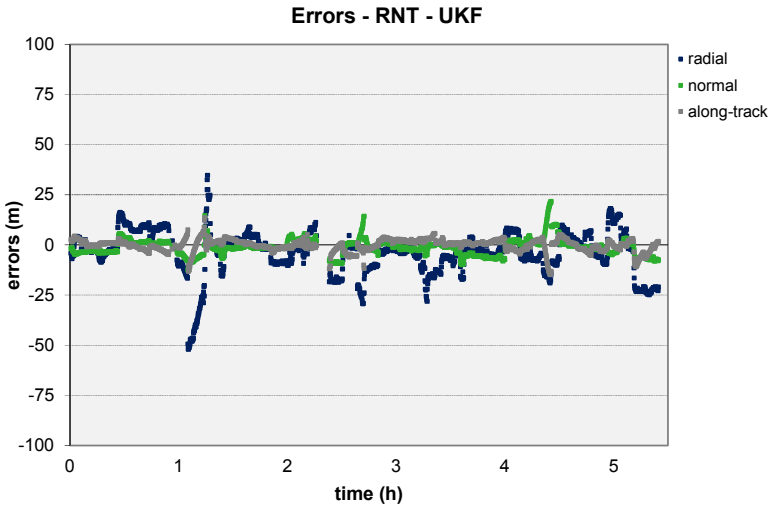

Figure 3. Errors in RNT coordinates, for the UKF simulation.

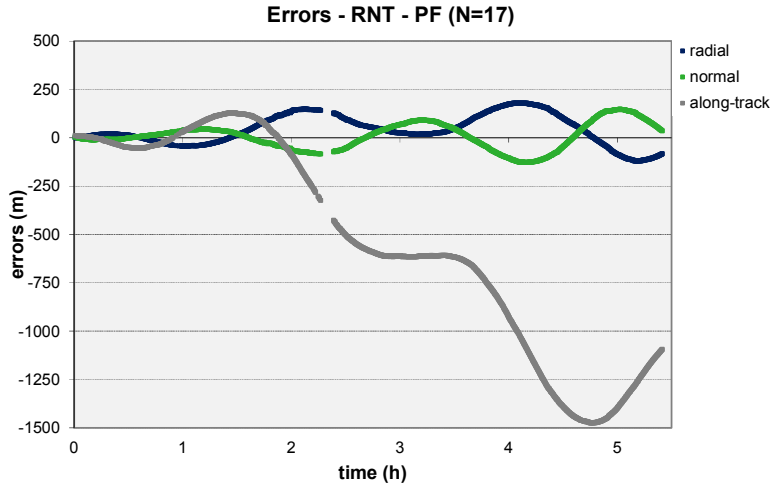

Figure 4. Errors in RNT coordinates, for the PF ($N = 17$) simulation.

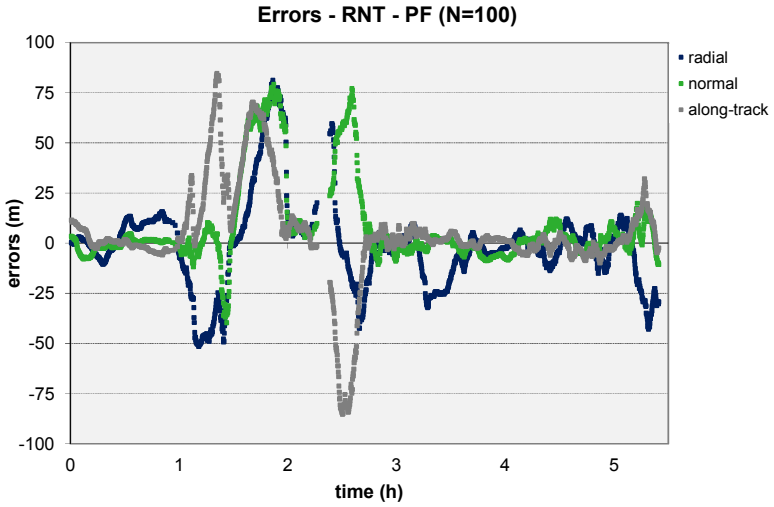

Figure 5. Errors in RNT coordinates, for the PF (N = 100) simulation.

In order to properly evaluate the PF (N = 500) performance, two other graphics were generated. Figures 6 and 7 present Δr and Δv (errors in position and velocity), respectively, where the results obtained in the PF (green curves) are compared with the UKF (dark blue curves). According to the results, it is clear that this version of the PF is as competitive as the UKF, in terms of accuracy. This means that the PF was correctly implemented and, from now, it is necessary to tune it more adequately. It also depends on the knowledge about the PF variants and, as said before, these results are the authors' first experiment with this issue. In each Figure, Δr and Δv represent, respectively, the absolute value of the errors in position and in velocity, in the ECEF (Earth-Centered Earth-Fixed) reference frame, also known as ECR (Earth-Centered Rotational).

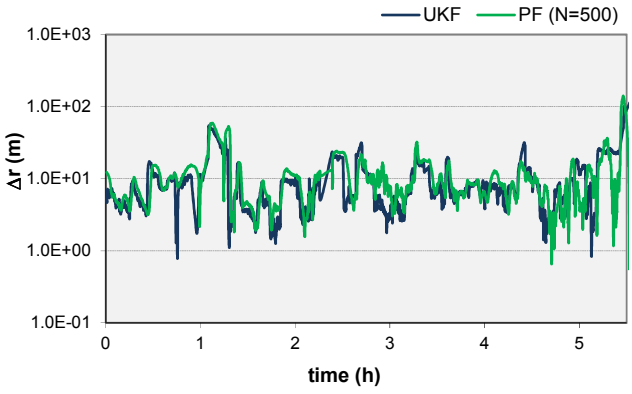

Figure 6. Δr obtained in the PF (N = 500) and the UKF simulations.

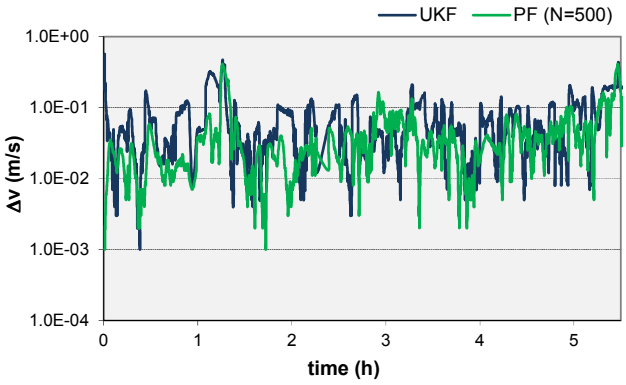

Figure 7. Δv obtained in the PF (N = 500) and the UKF simulations.

CONCLUSIONS

A Bayesian bootstrap filter algorithm was applied for the satellite orbit determination problem, using a set of GPS measurements. The development was evaluated through performance and computational cost, comparing the bootstrap algorithm results and the UKF solution for the same problem. The PF was implemented with resampling and roughening.

Regarding time of processing, results showed that the time required for the PF algorithm is greater than the UKF. As for the PF the number of particles is chosen as a trade-off between computational cost and estimation accuracy, the CPU time is directly related to the number of particles chosen only when the number of particles changes. There is no relation between time of processing and estimator implemented.

Results confirm that the greater the number of particles, the better the estimation accuracy. The best result was achieved by the UKF algorithm, and the PF closest performance was obtained in the PF (N=500) version. Even though a particular configuration of the PF has reached equivalent performance to the UKF, a high computational effort was demanded. As these results represent the PF first experiment and it has many variants, it can be tuned, likewise the Kalman filter.

In order to obtain better PF performance, especially in terms of estimation accuracy, adjusts in the many filter variants might be done, for improving its efficiency. Such adjusts are directly related to the knowledge about the filter. Procedures as prior editing can also be used to solve implementation issues such as sample impoverishment. Another approach for improving particle filtering is to combine it with another filter such as EKF or UKF. In this approach, each particle is updated at the measurement time using the EKF or the UKF, and then resampling is performed using the measurements.

ACKOWLEDGMENTS

The authors wish to express their consideration to the National Institute for Space Research (INPE) that kindly provided everything necessary for this paper to be developed. The authors are also grateful to National Council for Scientific and Technological Development (CNPq), for the support under contracts N. 160101/2012-3 and N. 303119/2010-1; and to São Paulo Research Foundation (FAPESP), for the support under contract N. 2012/21023-6.

REFERENCES

[1] R. van der Merwe, "Sigma-Point Kalman Filters for Probabilistic Inference in Dynamic State-Space Models", *Ph.D thesis*. Oregon Health & Science University, Portland, 2004.

[2] S.J. Julier, and J.K. Uhlmann, "A new extension of the Kalman filter for nonlinear systems". *International Symposium on Aerospace/Defense Sensing, Simulation and Controls*. SPIE, 1997.

[3] S.J. Julier, and J.K. Uhlmann, "Unscented filtering and nonlinear estimation". In: IEEE Transactions on Automatic Control, v. 92, n. 3, 2004. *Proceedings*… Mar 2004.

[4] D. Simon, *Optimal state estimation*. Wiley-Interscience, John Wiley & Sons, Inc., Hoboken, NJ, 2006. 526 p.

[5] N.J. Gordon, D.J. Salmond, A.F.M. Smith, "Novel approach to nonlinear/non-Gaussian Bayesian state estimation". IEE Proceedings-F, v. 140, n. 2, p. 107-113, April 1993.

[6] P.C.P.M. Pardal, H. K. Kuga, and R. Vilhena de Moraes, "Robustness Assessment between Sigma Point and Extended Kalman Filter for Orbit Determination". *Journal of Aerospace Engineering, Sciences and Applications*, v. III, p. 35-44, 2011.

[7] P.C.P.M. Pardal, H. K. Kuga, and R. Vilhena de Moraes, "A Discussion Related to Orbit Determination Using Nonlinear Sigma Point Kalman Filter". *Mathematical Problems in Engineering*, v. 2009, 12 p. Hindawi Publishing Corporation, doi:10.1155/2009/140963.

[8] D.-J. Lee and K.T. Alfriend, "Precise real-time satellite orbit estimation using the unscented Kalman filter". *AAS/AIAA Space Flight Mechanics*. AAS 03-230, pp. 853-1872. Advances in the Astronautical Sciences, Ponce, Puerto Rico, 2003.

[9] E. A. Wan, and R. van der Merwe, 2001, "The unscented Kalman filter". *Kalman Filtering and Neural Networks*. Haykins, S. (Ed.), John Wiley & Sons, New York, Chap. 7.

[10] P.S. Maybeck, *Stochastic models, estimation, and control*. v. 2, Academic Press, NY, 1982.

[11] R.G., Brown, and P.Y.C. Hwang, A Kalman filter approach to precision GPS geodesy. *Navigation: Global Positioning System*, v. II, p. 155-166, 1984.

[12] O. Montenbruck, and E. Gill, *Satellite Orbits: models, methods, and applications*. Springer-Verlag, Berlin Heidelberg NewYork, 2001. 369p.

[13] R.G., Brown, and P.Y.C. Hwang, *Introduction to random signals and applied Kalman filtering*. 3rd. ed. New York: John Wiley & Sons, 1985. 502p.

[14] W.M. Kaula, *Theory of Satellite Geodesy*. Blasdell Pub. Co. Walthmam, Mass, 1966.

[15] JASON-2: Altimetry mission for ocean observation.URL: smsc.cnes.fr/JASON2.

[16] P.W. Binning, "GPS, Dual Frequency, SA Free Satellite Navigation. Navigation Technology for the 3rd Millennium". In: 52nd Annual Meeting of the Institute of Navigation, p. 803-812. Cambridge, MA, USA: 19-21 June, 1996. *Proceedings*…

[17] J.A. Marshall, and S.B. Luthcke, "Modeling Radiation Forces on Topex/Poseidon for Precision Orbit Determination". *Journal of Spacecraft and Rockets*, vol. 31, n. 1, Jan. - Feb., 1994.

[18] A.F.B.A. Prado, and H.K. Kuga (Eds), *Fundamentos de Tecnologia Espacial*. São José dos Campos: INPE, 2001. 220 p. ISBN: 85-17-00004-8.

[19] T. Guan, "Special cases of the three body problem". [online Colorado University database], URL: http://inside.mines.edu/fs_home/tohno/teaching/PH505_2011/Paper_TianyuanGuan.pdf.

[20] A.P.M. Chiaradia, H.K. Kuga, and A.F.B.A. Prado, "Single frequency GPS measurements in real-time artificial satellite orbit determination". *Acta Astronautica*, v. 53, n. 2, p. 123-133, 2003.

[21] "OSTM/Jason-2 Products Handbook". 67p. 03 Aug. 2009. [online JPL/NASA database], URL: ftp://podaac.jpl.nasa.gov/allData/ostm/preview/L2/GPS-OGDR/docs/userhandbook.pdf.

[22] P.C.P.M. Pardal, H. K. Kuga, and R. Vilhena de Moraes, "Comparing the Extended and the Sigma Point Kalman Filters for Orbit Determination Modeling Using GPS Measurements". In: 23rd International Meeting of the Satellite Division of the Institute of Navigation (ION GNSS 2010), p. 2732-2742. 21-24 Sept., Portland, USA. *Proceedings*…

[23] P.C.P.M. Pardal, "Determinação de Órbita em Tempo Real Através de Filtro Não Linear de Kalman Sigma-Ponto", *Ph.D thesis*. National Institute for Space Research (INPE), São José dos Campos, 2011. 138p.